Modélisation numérique d'un système couplé fluide structure en présence d'effets de ballottement et de capillarité

Quentin Akkaoui, Evangéline Capiez-Lernout, Christian Soize, Roger Ohayon

Computational modeling of a coupled fluid-structure system with sloshing and capillarity

Q. AKKAOUI[a], E. CAPIEZ-LERNOUT[a], C. SOIZE[a], R. OHAYON[b]

a. Laboratoire Modélisations et Simulations Multi Echelles (MSME) UMR 8208 CNRS,
5 Boulevard Descartes 77454 Marne-La-Vallée, France
quentin.akkaoui@u-pem.fr
evangeline.capiez-lernout@univ-paris-est.fr
christian.soize@univ-paris-est.fr
b. Structural Mechanics and Coupled System Laboratory, Conservatoire National des Arts et Métiers (CNAM), 2 rue Conte, 75003, Paris , France
roger.ohayon@cnam.fr

Résumé :

Ce papier propose une approche numérique pour l'étude en vibro-acoustique interne d'une structure élastique dissipative linéaire couplée à un fluide acoustique linéaire en présence des effets de ballottement et de capillarité. Ce travail est basé sur une nouvelle formulation pour la condition aux limites d'angle de contact sur la ligne triple. Un modèle réduit est construit en utilisant une base de projection constitué de modes élastiques, de modes acoustiques et de modes de ballottement en présence de capillarité. Une application numérique est présentée.

Abstract :

This paper is devoted to a numerical approach in vibroacoustics of a linear elastic structure coupled with a compressible liquid with sloshing and capillarity effects. This work is based on a new formulation for the boundary condition on the contact angle. A reduced-order model is constructed using a projection basis made up of elastic modes, acoustic modes, and sloshing-capillarity modes. Then a numerical study of a coupled fluid-structure system discretized with finite element modeling is presented.

Key words : Fluid-structure interactions, sloshing, capillarity, contact angle, reduced-order model.

1 Introduction

This paper deals with the computational analysis of a coupled fluid-structure system under sloshing and capillarity effects for which the response of the system is assumed to remain in a linear domain. The damped elastic structure under consideration contains a linear dissipative acoustic liquid for which sloshing and capillarity effects due to gravity and surface tensions are taken into account. Many researches have been performed concerning the formulation and the analysis of coupled fluid-structure systems. For

instance, the sloshing phenomenon has been studied by considering an elastic structure coupled with an incompressible fluid neglecting the capillarity effects (see for instance [9, 10, 2, 11, 8, 4, 14]), by considering a rigid structure coupled with an incompressible fluid with capillarity effects [10, 3]. Other works have been done considering a rigid structure coupled with a compressible liquid under surface tension and sloshing effects such as [1, 5, 6, 7]. More recently, a new theoretical formulation of a linear reduced-order computational model for analyzing the linear vibrations of a linear viscoelastic structure coupled with a linear dissipative acoustic liquid with sloshing and capillarity effects has been proposed [13] for which the main novelty concerns the implementation of a new boundary condition for the contact angle and the computation of a reduced-order model that is constructed using a projection basis constituted of the elastic modes of the structure with a fluid added mass effect, the acoustic modes of the fluid, and the sloshing-capillarity modes of the free-surface of the fluid. We refer the reader to [12, 13] for the methodology related to the construction of the vector basis. In this work, we present the computational implementation of this theoretical formulation for which the structure is simply dissipative (not viscoelastic). In Section 2, the boundary value problem that describes the coupled fluid-structure system is presented. The finite element discretization and the methodology for constructing the reduced-order model is given in Section 3. Section 4 deals with the numerical application, for which the vibroacoustic analysis is presented in details using such new computational reduced-order model.

2 Boundary value problem

We consider the linear coupled fluid-structure system in its reference configuration defined in Figure 1. The dissipative structure Ω_S is linear elastic and contains a linear dissipative acoustic fluid, Ω_L. Gravitational and surface tension effects are taken into account. The boundaries $\partial\Omega_S$ and $\partial\Omega_L$ are such as $\partial\Omega_S = \Gamma_E \cup \Gamma_L \cup \gamma \cup \Gamma_G$ and $\partial\Omega_L = \Gamma_L \cup \gamma \cup \Gamma$, where Γ_E, Γ_L, Γ_G, Γ and γ are, respectively, the external surface of the structure, the fluid-structure interface, the internal surface of the structure without contact with the liquid, the free surface of the liquid, and the contact line between Γ and Γ_L (see Figure 1). The structure is submitted to a given body force field $\mathbf{b}$ in Ω_S and to a given surface force field $\mathbf{f}$ on Γ_E. The external unitary normals to $\partial\Omega_S$ and $\partial\Omega_L$ are written $\mathbf{n}^S$ and $\mathbf{n}$. Let $\boldsymbol{\nu}$ and $\boldsymbol{\nu}_L$ be the external unit normals to γ belonging respectively to the tangent plane to Γ and to the tangent plane to Γ_L. We are then interested in analyzing the vibrations of the coupled fluid-structure system around its reference configuration.

Let $\mathbf{x} = (x, y, z)$ be the generic point in a Cartesian reference system $(\mathbf{O}, \mathbf{e}_x, \mathbf{e}_y, \mathbf{e}_z)$. The gravity vector is $\mathbf{g} = -g\,\mathbf{e}_z$ with $g = \|\mathbf{g}\|$. For a quantity w depending on time t, $\dot{w}$ and $\ddot{w}$ mean the first and the second partial derivative of w with respect to t. The boundary value problem is expressed in terms of the structural displacement field $\mathbf{u}(\mathbf{x}, t)$, the internal pressure field $p(\mathbf{x}, t)$, and the normal displacement field of the free surface $\eta(\mathbf{x}, t)$,

$$\frac{1}{\rho_0 c_0^2}\,\ddot{p} - \frac{\tau}{\rho_0}\nabla^2\dot{p} - \frac{1}{\rho_0}\nabla^2 p = 0 \quad \text{in } \Omega_L\ , \tag{2.1}$$

$$(1 + \tau\frac{\partial}{\partial t})\,\frac{\partial p}{\partial \mathbf{n}} = -\rho_0 \ddot{\mathbf{u}}\cdot\mathbf{n} \quad \text{on } \Gamma_L\ , \tag{2.2}$$

$$(1 + \tau\frac{\partial}{\partial t})\,\frac{\partial p}{\partial \mathbf{n}} = -\rho_0 \ddot{\eta} \quad \text{on } \Gamma\ , \tag{2.3}$$

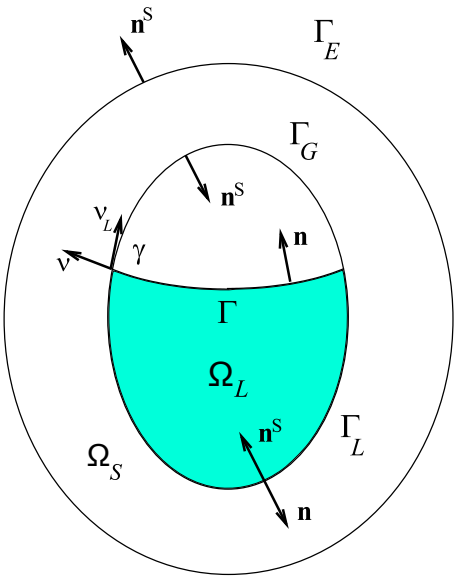

Figure 1 – Reference configuration of the coupled fluid-structure system

$$p = \rho_0\,\eta\,g\,(\mathbf{e}_z\cdot\mathbf{n}) - \sigma_\Gamma\{(\frac{1}{R_1}+\frac{1}{R_2})\eta + \nabla^2_\Gamma\eta\} \quad \text{on } \Gamma\ , \tag{2.4}$$

$$\frac{\partial\eta}{\partial\boldsymbol{\nu}} = c_\eta\eta + \mathcal{J}\mathbf{u} \quad \text{on } \gamma\ , \tag{2.5}$$

$$\rho_s\,\ddot{\mathbf{u}} - \text{div}\,\boldsymbol{\sigma} = \mathbf{b} \quad \text{in } \Omega_S\ , \tag{2.6}$$

$$\boldsymbol{\sigma}\cdot\mathbf{n}^S = \mathbf{f} \quad \text{on } \Gamma_E\ , \tag{2.7}$$

$$\boldsymbol{\sigma}\cdot\mathbf{n}^S\,d\Gamma_L = p\,\mathbf{n}^S\,d\Gamma_L - \sigma_\Gamma\,(\mathcal{J}'\eta)\,d\mu_\gamma \quad \text{on } \Gamma_L\ , \tag{2.8}$$

in which ρ_0 is the constant mass density of the homogeneous liquid, c_0 is the constant speed of sound, τ is the constant coefficient that characterizes the dissipation in the internal liquid, ρ_S is the constant mass density of the structure, $\boldsymbol{\sigma} = \mathbb{a} : \varepsilon(\mathbf{u}) + \mathbb{b} : \varepsilon(\dot{\mathbf{u}})$ is the stress tensor in which ε the linearized strain tensor, g is the gravitational intensity, σ_Γ is the surface tension coefficient, R_1 and R_2 are the main curvature radii of the free-surface and c_η is the contact angle coefficient. Equations (2.5) and (2.8) correspond to a new boundary condition for the contact angle introduced in [13] in which a particular case for the operator $\mathcal{J}$ is given by [10],

$$\mathcal{J}\mathbf{u} = E\,\mathbf{u}\cdot\mathbf{n}^S - \frac{\partial(\mathbf{u}\cdot\mathbf{n}^S)}{\partial\boldsymbol{\nu}_L}\,, \tag{2.9}$$

with E a real coefficient. In Eq. (2.8), $d\mu_\gamma$ is a real measure on Γ_L such that $\int_{\Gamma_L} f(\mathbf{x})\,d\mu_\gamma(\mathbf{x}) = \int_\gamma f(\mathbf{x})\,d\gamma(\mathbf{x})$ (this means that the support of measure $d\mu_\gamma$ is γ), and the term $(\mathcal{J}'\eta)\,d\mu_\gamma$ is defined on Γ_L by algebraic duality of the term $\mathcal{J}\mathbf{u}$ defined on γ.

3 Computational model

Let $\mathbf{P}(t)$, $\mathbf{H}(t)$, and $\mathbf{U}(t)$ be the $(n_F\times 1)$, $(n_H\times 1)$, and $(n_S\times 1)$ vectors (column matrices) corresponding to the finite element discretization of the fields $p(\mathbf{x},t)$, $\eta(\mathbf{x},t)$, and $\mathbf{u}(\mathbf{x},t)$. The computational model

associated with boundary value problem is written as,

$$[M]\,\ddot{\mathbf{P}}(t) + [D]\,\dot{\mathbf{P}}(t) + [K]\,\mathbf{P}(t) - [C_{p\eta}]^T\,\ddot{\mathbf{H}}(t) - [C_{pu}]^T\,\ddot{\mathbf{U}}(t) = 0\,, \tag{3.1}$$

$$[C_{p\eta}]\,\mathbf{P}(t) + ([K_g] + [K_c])\mathbf{H}(t) + [C_{\eta u}]\,\mathbf{U}(t) = 0\,, \tag{3.2}$$

$$[C_{pu}]\,\mathbf{P}(t) + [C_{\eta u}]^T\,\mathbf{H}(t) + [M_S]\,\ddot{\mathbf{U}}(t) + [D_S]\,\dot{\mathbf{U}}(t) + [K_S]\,\mathbf{U}(t) = \mathbf{F}^S(t)\,, \tag{3.3}$$

in which $[M]$, $[D]$, $[K]$ and $[M_S]$, $[D_S]$, $[K_S]$ are the mass, dissipation and stiffness matrices for the acoustic fluid and for the structure, where $[C_{pu}]$ is the coupling matrix between the fluid and the structure, where $[C_{\eta u}]$ is the coupling matrix between the free surface of the liquid and the structure, where $[C_{p\eta}]$ is the coupling matrix between the fluid and the free surface, and where $[K_c]$ and $[K_g]$ are the stiffness matrices of the free surface induced by the gravitational and the capillarity effects [13].

4 Reduced-order model

4.1 Construction of the projection vector basis

The construction of the reduced-order model requires the computation of a vector basis made up of acoustic modes of the fluid, sloshing modes of the free surface, and elastic modes of the structure with the fluid added mass effect, as follows,

- The structural modes are calculated by solving the following generalized eigenvalue problem,

$$[K_S]\,\boldsymbol{\phi}^S_\alpha = \lambda^S_\alpha\,([M_S] + [M^A])\,\boldsymbol{\phi}^S_\alpha\,, \tag{4.1}$$

  in which the positive-definite symmetric matrix $[M^A]$ is the fluid added mass matrix that describes the effects of the liquid (assumed to be incompressible) on the structure [10, 13]. Let $[\,\Phi^S\,] = [\boldsymbol{\phi}^S_1, \ldots, \boldsymbol{\phi}^S_{N_S}]$ be the rectangular real matrix whose columns are the N_S eigenvectors associated with the N_S first smallest real positive eigenvalues $0 < \lambda^S_1 \leq \ldots \leq \lambda^S_{N_S}$.

- The acoustic modes of the fluid are computed by solving the generalized eigenvalue problem,

$$[K]\,\boldsymbol{\phi}^F_\beta = \lambda^F_\beta\,[M]\,\boldsymbol{\phi}^F_\beta\,, \tag{4.2}$$

  with the constraint $\boldsymbol{\phi}^F_\beta = 0$ for the DOF related to $\Gamma \cup \gamma$. Let $[\,\Phi^F\,] = [\boldsymbol{\phi}^F_1, \ldots, \boldsymbol{\phi}^F_{N_F}]$ be the rectangular real matrix whose columns are the N_F eigenvectors associated with the N_F first smallest real positive eignevalues $0 < \lambda^F_1 \leq \ldots \leq \lambda^F_{N_F}$.

- The sloshing-capillarity modes are computed by solving the generalized eigenvalue problem,

$$[K]\,\boldsymbol{\phi}^{FH}_\gamma + \lambda^H_\gamma\,[C_{p\eta}]^T\,\boldsymbol{\phi}^H_\gamma = 0\,, \tag{4.3}$$

$$[C_{p\eta}]\,\boldsymbol{\phi}^{FH}_\gamma + ([K_g] + [K_c])\,\boldsymbol{\phi}^H_\gamma = 0\,. \tag{4.4}$$

  Let $[\,\Phi^H\,] = [\boldsymbol{\phi}^H_1, \ldots, \boldsymbol{\phi}^H_{N_H}]$ and $[\,\Phi^{FH}\,] = [\boldsymbol{\phi}^{FH}_1, \ldots, \boldsymbol{\phi}^{FH}_{N_H}]$ be the rectangular real matrices whose columns are the N_H eigenvectors $\boldsymbol{\phi}^H_\gamma$ and the N_H eigenvectors $\boldsymbol{\phi}^{FH}_\gamma$ associated with the N_H first smallest real positive eigenvalues $0 < \lambda^H_1 \leq \ldots \leq \lambda^H_{N_H}$.

4.2 Reduced-order model

The reduced-order model of the coupled fluid-structure system of order (N_F, N_H, N_S) is written as,

$$\mathbb{X}(t) = \begin{bmatrix} \mathbf{P}(t) \\ \mathbf{H}(t) \\ \mathbf{U}(t) \end{bmatrix} = [\,\mathbf{\Phi}\,]\,\mathbf{Q} \quad , \quad [\,\mathbf{\Phi}\,] = \begin{bmatrix} [\Phi^F] & [\Phi^{FH}] & 0 \\ 0 & [\Phi^H] & 0 \\ 0 & 0 & [\Phi^S] \end{bmatrix} \quad , \quad \mathbf{Q} = \begin{bmatrix} \mathbf{q}^P(t) \\ \mathbf{q}^H(t) \\ \mathbf{q}^U(t) \end{bmatrix} , \tag{4.5}$$

in which $\mathbf{Q}$ is the $(N_F + N_H + N_S) \times 1$ vector (column matrix) of the generalized coordinates, which verifies the dynamical equation

$$[\mathcal{M}_{FSI}]\,\ddot{\mathbf{Q}} + [\mathcal{D}_{FSI}]\,\dot{\mathbf{Q}} + [\mathcal{K}_{FSI}]\,\mathbf{Q} = \mathcal{F}, \tag{4.6}$$

in which $[\mathcal{M}_{FSI}]$, $[\mathcal{D}_{FSI}]$, and $[\mathcal{K}_{FSI}]$ are the mass, the damping, and the stiffness matrices of order (N_F, N_H, N_S) of the coupled fluid-structure system such that

$$[\mathcal{M}_{FSI}] = [\,\mathbf{\Phi}\,]^T \begin{bmatrix} [M] & -[C_{p\eta}]^T & -[C_{pu}]^T \\ 0 & 0 & 0 \\ 0 & 0 & [M_S] \end{bmatrix} [\,\mathbf{\Phi}\,], \tag{4.7}$$

$$[\mathcal{D}_{FSI}] = [\,\mathbf{\Phi}\,]^T \begin{bmatrix} [D] & 0 & 0 \\ 0 & 0 & 0 \\ 0 & 0 & [D_S] \end{bmatrix} [\,\mathbf{\Phi}\,], \tag{4.8}$$

$$[\mathcal{K}_{FSI}] = [\,\mathbf{\Phi}\,]^T \begin{bmatrix} [K] & 0 & 0 \\ [C_{p\eta}] & [K_g] + [K_c] & [C_{\eta u}] \\ [C_{pu}] & [C_{\eta u}]^T & [K_S] \end{bmatrix} [\,\mathbf{\Phi}\,], \tag{4.9}$$

and where $\mathcal{F}$ is the $(N_F + N_H + N_S) \times 1$ vector (column matrix) of the generalized forces defined by

$$\mathcal{F} = [\,\mathbf{\Phi}\,]^T \begin{bmatrix} 0 \\ 0 \\ \mathbf{F}^S(t) \end{bmatrix} . \tag{4.10}$$

5 Numerical application

5.1 Finite element model of the coupled fluid-structure system

The coupled fluid-structure system is composed of a spherical tank with external radius $R_e = 0.5\,m$ and thickness $e = 2.3 \times 10^{-2}\,m$, partially filled with an acoustic fluid. The origin $\mathbf{O}$ of the Cartesian coordinates system $(\mathbf{O}, \mathbf{e}_x, \mathbf{e}_y, \mathbf{e}_z)$ is located at the center of the spherical tank. The structure is made up of a linear elastic isotropic material with mass density $\rho_S = 1650\,Kg \times m^{-3}$, Poisson coefficient $\nu = 0.3$, and Young's modulus $E = 230\,GPa$. The considered liquid is water in standard temperature and pressure conditions, with mass density $\rho_f = 1000\,Kg \times m^{-3}$, speed of sound $c_f = 1480\,m \times s^{-1}$, surface tension coefficient $\sigma_\Gamma = 0.0728$, and contact angle $\alpha = 30^\circ$. The main curvature radii R_1 and R_2 of the free surface and the coefficients c_η and E, which characterizes the triple line γ, are computationally obtained in each node of the mesh according to [10]. The damping matrices of the acoustic fluid and the structure are defined as $[D] = \tau_F\,[K]$ and $[D_S] = \tau_S\,[K_S]$ in which $\tau_F = 10^{-6}$ and $\tau_S = 10^{-6}$.

The spherical tank is clamped on a ring shaped support such that $z \in [-0.375\,,-0.475]\,m$. The finite element model of the coupled fluid structure system is constructed using 3D solid finite elements with 8 nodes for the structure and the acoustic fluid, 2D finite elements with 4 nodes for the free-surface and 1D finite elements with 2 nodes for the triple line γ. Table 1 gives the values of the parameters that correspond to the finite element model displayed in Figure 2.

Parameters	**Nodes**	**DOF**	**Finite elements**	**Type of element**
Structure	5,812	17,436	2,904	3D
Fluid	27,482	27,482	25,828	3D
Free surface	1,673	1,673	1,628	2D
Triple line	88	88	44	1D

Table 1 – Values of the parameters of the the finite element model

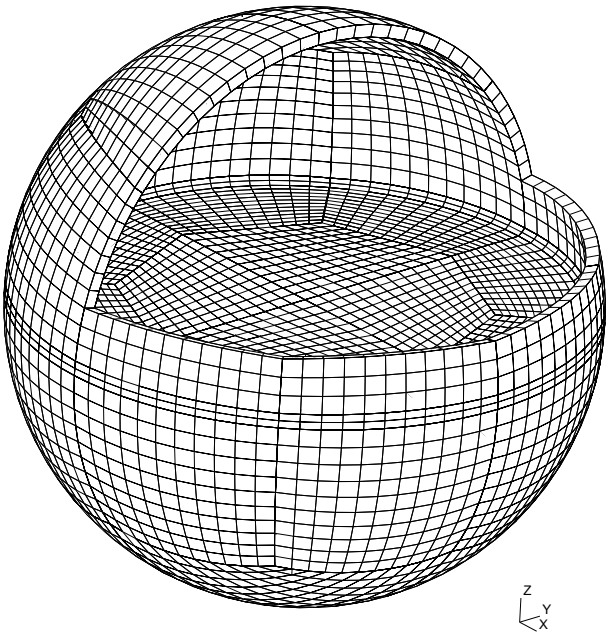

Figure 2 – Finite element mesh of the coupled fluid-structure system

5.2 Modal characterization of the fluid-structure system

To better understand the physical mechanisms that control the vibrational behavior of the coupled fluid-structure system, we are interested in representing some modal contributions issued from the projection basis used for constructing the reduced-order model. Figure 3 displays the shape of 3 structural elastic modes $\boldsymbol{\phi}_1^S$, $\boldsymbol{\phi}_3^S$, and $\boldsymbol{\phi}_8^S$ associated with the eigenfrequencies $\nu_1^S = 655\,Hz$, $\nu_3^S = 1{,}717\,Hz$, and $\nu_8^S = 3{,}042\,Hz$. Figure 4 displays the pressure field of 3 acoustic modes $\boldsymbol{\phi}_1^F, \boldsymbol{\phi}_4^F$, and $\boldsymbol{\phi}_8^F$ associated with the eigenfrequencies $\nu_1^F = 985\,Hz$, $\nu_3^F = 2{,}160\,Hz$, and $\nu_8^F = 2{,}708\,Hz$. The modal shape of these pure structural and acoustic modes are suitable for observing elasto-acoustic coupling when analyzing the coupled fluid-structure system. For instance, since ν_1^S and ν_1^F are close eigenfrequencies whose modal shapes $\boldsymbol{\phi}_1^S$ and $\boldsymbol{\phi}_1^F$ do not cancel each other out, they are likely to be coupled. It can be seen that there are global and local sloshing modes. Nevertheless, a careful attention has to be made regarding the selection of these modes because of the precision of the finite element mesh allowing the modal shapes of these modes to be correctly represented. Figure 5 displays the shape of 6 sloshing-capillarity

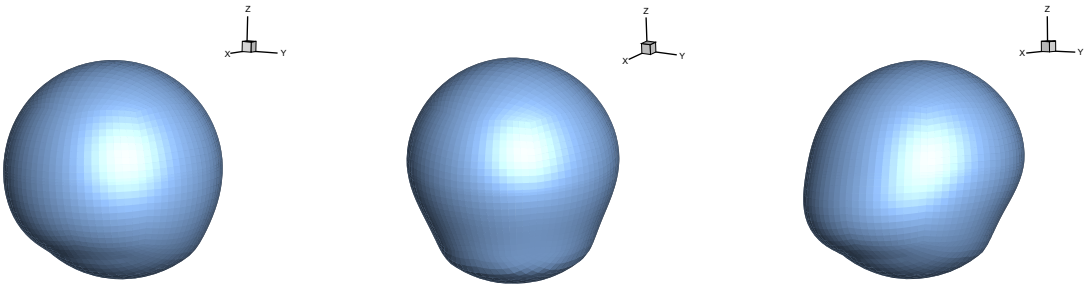

$\nu_1^S = 655\,Hz$ $\nu_3^S = 1{,}717\,Hz$ $\nu_8^S = 3{,}042\,Hz$

Figure 3 – Example of elastic modes of the structure.

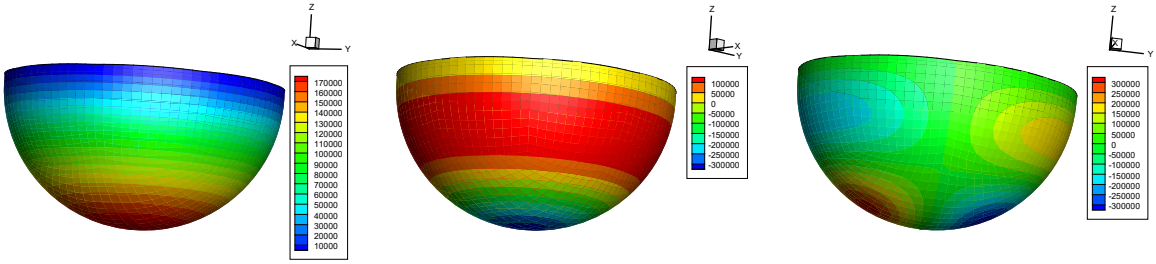

$\nu_1^F = 985\,Hz$ $\nu_3^F = 2{,}160\,Hz$ $\nu_8^F = 2{,}708\,Hz$

Figure 4 – Example of acoustic modes of the fluid.

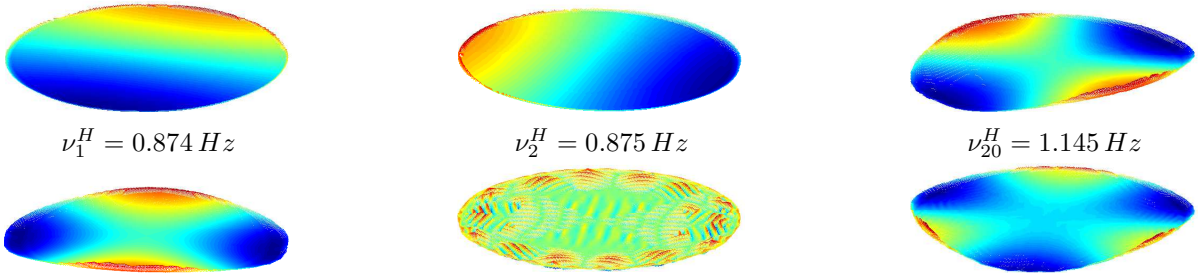

$\nu_1^H = 0.874\,Hz$ $\nu_2^H = 0.875\,Hz$ $\nu_{20}^H = 1.145\,Hz$

$\nu_{21}^H = 1.148\,Hz$ $\nu_{83}^H = 1.328\,Hz$ $\nu_{87}^H = 1.330\,Hz$

Figure 5 – Example of sloshing modes of the free surface.

modes ϕ_1^H, ϕ_2^H, ϕ_{20}^H, ϕ_{21}^H, ϕ_{83}^H, and ϕ_{87}^H associated with the eigenfrequencies $\nu_1^H = 0.874\,Hz$, $\nu_2^H = 0.875\,Hz$, $\nu_{20}^H = 1.145\,Hz$, $\nu_{21}^H = 1.148\,Hz$, $\nu_{83}^H = 1.328\,Hz$, and $\nu_{87}^H = 1.330\,Hz$.

5.3 Forced responses

5.3.1 Definition of the time dependent external force

We are interested in analyzing the forced response of the coupled fluid-structure system formulated both in the time domain and in the frequency domain. The structure is submitted to an external force defined in the time domain such that its energy is concentrated in the frequency band $\mathbb{B}_e = [\nu_{\min}, \nu_{\max}]$. In this numerical analysis, we have chosen $\nu_{\min} = 600\,Hz$ and $\nu_{\max} = 6{,}000\,Hz$. The external load vector

$\mathbf{F}^S(t)$ is written as

$$\mathbf{F}^S(t) = f_0\, g(t)\, \mathbb{F}\,,$$

in which f_0 is a real coefficient controlling the intensity of the force, $\mathbb{F}$ is the $(n_S \times 1)$ normalized vector that describes the spatial discretization of the force, and where $g(t)$ is the function describing the time evolution of the force such that

$$g(t) = 2\,\Delta\nu\, \frac{\sin(\pi t\, \Delta\nu)}{\pi t\, \Delta\nu}\, \cos(2\pi s\, \Delta\nu\, t)\,, \tag{5.1}$$

with

$$\Delta\nu = \nu_{\max} - \nu_{\min} \quad , \quad s = \frac{1}{2}\frac{\nu_{\max} + \nu_{\min}}{\Delta\nu}\,. \tag{5.2}$$

The external force is a normal force that is applied to the spherical cap located from $z = 0.437\,m$ to the top, with a force intensity $f_0 = 1{,}200\,N$. Figure 6 displays the graph of the function $t \mapsto g(t)$ and its Fourier transform $\nu \mapsto \widehat{g}(2\pi\nu)$. It can be viewed that this choice of $g(t)$ effectively yields an uniform excitation over frequency band $\mathbb{B}_e$. Let $\mathbb{B} = \mathbb{B}_e$ be the frequency band of analysis of the fluid-

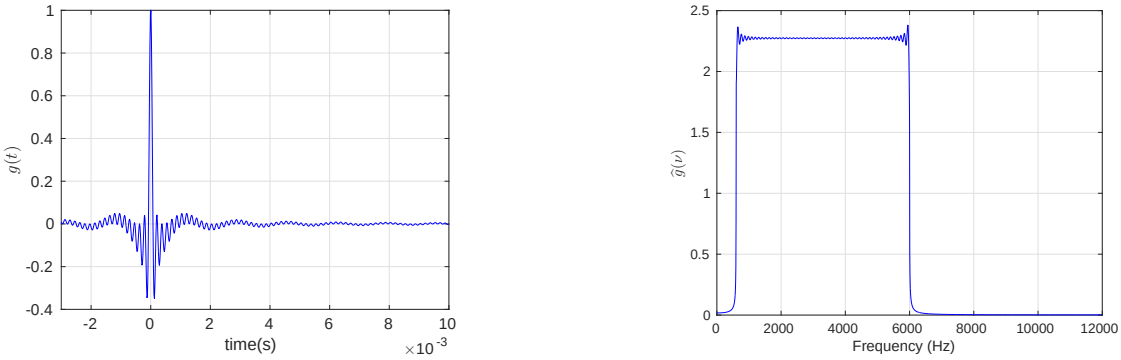

Figure 6 – Representation of the external force in the time domain and in the frequency domain: graph of $t \to g(t)$ (left figure) and graph of $\nu \to \widehat{g}(2\pi\nu)$ (right figure) for frequency band $\mathbb{B}_e = [600\,Hz\,,\, 6\,000\,Hz]$

structure system. This linear dynamical analysis is performed in the time domain using the Newmark time-integration scheme. The Fourier transform of the times responses are computed in order to analyze the response in the frequency domain.

5.3.2 Convergence of the reduced-order model

The optimal number of modes (N_F, N_H, N_S) to be kept in the reduced-order model can be obtained by a convergence analysis of the dynamical responses. Let $\widehat{\mathbb{X}}_{ref}(\nu)$ be the dynamical response in the frequency domain of the computational model of the fluid-structure system, which is considered as the reference system. Let $\widehat{\mathbb{X}}(\nu)$ be the corresponding dynamical response calculated with the reduced-order model. We then define the function $(N_F, N_H, N_S) = \text{Conv}(N_F, N_H, N_S)$ by

$$\text{Conv}(N_F, N_H, N_S) = \frac{1}{||\widehat{\mathbb{X}}_{ref}(\nu)||^2} \int_{\mathbb{B}} ||\, \widehat{\mathbb{X}}(\nu, N_F, N_H, N_S)\, ||^2\, d\nu\,. \tag{5.3}$$

For the values $\{40, 60, 80, 100, 120\}$ of N_F, Figure 7 displays the graph of $N_S \mapsto \text{Conv}(N_F, 500, N_S)$, which shows that an optimal number of the elastic modes is $N_S = 70$ and an optimal number of the

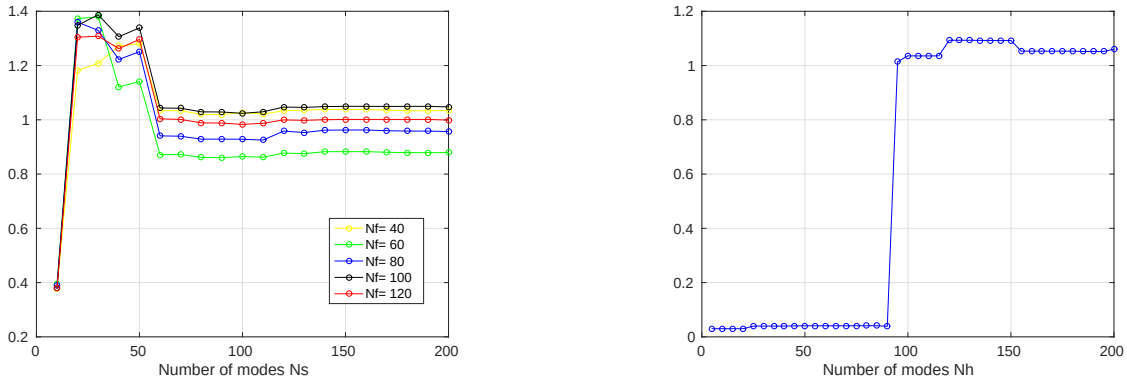

Figure 7 – Convergence analysis of the reduced-order model: graph of $N_S \mapsto \text{Conv}(N_F, 500, N_S)$ (left graph) and $N_H \mapsto \text{Conv}(100, N_H, 70)$ (right graph).

acoustic modes is $N_F = 100$. For such optimal values, the dynamical responses obtained with the reduced-order model are close to those given by the computational model that is the reference. Figure 7 (right graph) displays the graph of $N_H \mapsto \text{Conv}(100, N_H, 70)$ and shows that the dynamical behavior of the coupled fluid-structure system is correctly represented by the reduced-order model of order $(N_F, N_H, N_S) = (100, 150, 70)$.

5.3.3 Observation points

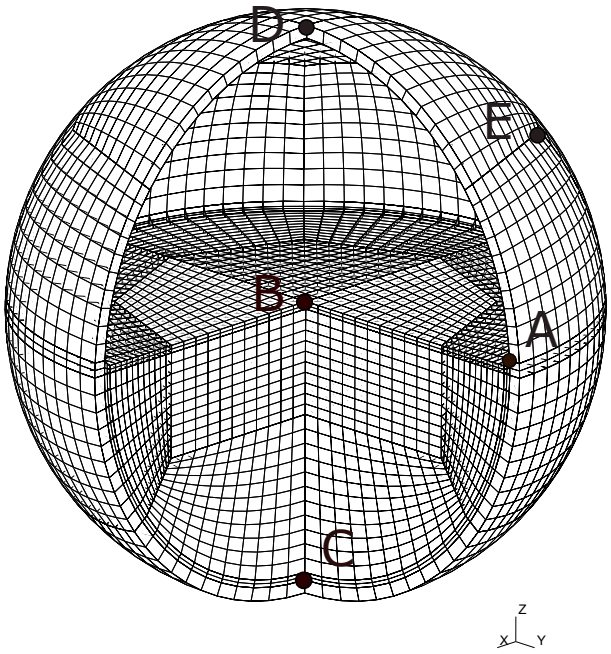

Figure 8 – Observation points of the fluid-structure system

Figure 8 displays the observation points for the structure, the fluid, and the free-surface, for which the dynamical response in terms of displacement, pressure, and elevation is shown hereinafter. Point A is an observation point common to the fluid, the structure, and the free surface located in γ. Point B is an observation point common to the fluid and the free surface located in Γ. Point C is an observation point for the fluid located in Γ_L, and points D and E are observation points for the structure located in Γ_E. The coordinates of the observation points are summarized in Table 2. We then denote the observation points

of the structure as $n^S_{obs} = (1, 2, 3)$, the observation points for the pressure in the fluid as $n^F_{obs} = (1, 2, 3)$, and the observation points for the elevation of the free surface $n^H_{obs} = (1, 2, 3)$.

Point	Coordinates	Fluid	Free surface	Structure
Point 1	x_1	0	0	0
	y_1	0.476	0.476	0
	z_1	0.025	0.025	0.5
Point 2	x_2	0	0	0
	z_2	0	0	0.476
	x_2	0.013	0.013	0.025
Point 3	x_3	0	0.33	-0.337
	y_3	0	-0.33	-0.337
	z_3	-0.477	0.018	0.15

Table 2 – Coordinates of the observation points for the fluid, the structure and the free surface

5.4 Dynamic analysis of the coupled fluid-structure system

For the observation points described in the previous section, Figures 9, 10, and 11 display the graphs of the time dynamical responses in terms of displacement of the structure, the pressure in the fluid, and the elevation of the free surface. Figures 12, 13, and 14 display the similar graphs of the frequency dynamical responses. In Figure 9, it can be seen that the displacement related to observation point 1 of the structure is mainly along $\mathbf{e}_z$ since the external force is normal to the spherical tank. It can also be seen that the displacement at observation point 3 of the structure is more damped than the displacement at observation point 2 of the structure. This can be explained by the coupling of the inertial contribution of the sloshing-capillarity modes on the structure, because observation point 2 is located in the contact line γ, where coupling effects are logically the most important. Moreover, in Figure 11, it can be seen that the elevation of the free surface is more damped in the contact line (observation point 1 on the free surface) than at the center (observation points 2 and 3 on the free surface), for which the capillarity effects are negligible. As expected when analyzing the modal shapes of the structure and the modal shapes of the fluid, elasto-acoustic resonances resulting from the coupling of these modes can be put in evidence in Figure 12, 13 and 14. The first resonance of the coupled fluid-structure system appears at $\nu_1 = 820\,Hz$ and results from the coupling between the first elastic mode $\boldsymbol{\phi}^S_1$ and the first acoustic mode $\boldsymbol{\phi}^F_1$. The second resonance of the coupled fluid-structure system appears at $\nu_2 = 1{,}441\,Hz$ and is also a coupling between the third elastic mode $\boldsymbol{\phi}^S_3$ and the third acoustic mode $\boldsymbol{\phi}^F_3$. Note that the fourth resonance that occurs at $\nu_4 = 2{,}648\,Hz$ is a pure acoustic mode and the seventh resonance frequency $\nu_7 = 3{,}592\,Hz$ is a pure elastic mode. Furthermore, since the sloshing modes do not belong to the frequency band of analysis and occur at very low frequencies, only the inertial contributions are expected.

6 Conclusion

In this paper, the methodology is presented for the implementation of a computational reduced-order model that allows for analyzing the dynamic analysis of a coupled fluid-structure system under sloshing and capillarity effects in taking into account the operator related to the triple line. A numerical application is presented. The inherent mechanisms regarding the couplings between the dissipative acoustic liquid and the linear dissipative elastic structure are shown in order to better understand the vibrational behavior of the fluid-structure system under sloshing and surface tension effects. It is shown

that sloshing-capillarity effects are playing a role on the coupled fluid-structure system through its inertial part since the liquid sloshes at very low frequencies outside the frequency band of analysis. This research is a first step to a more complex dynamical analysis that is in progress for which the nonlinear geometrical effects of the structure induced by large displacements and large deformations are taken into account.

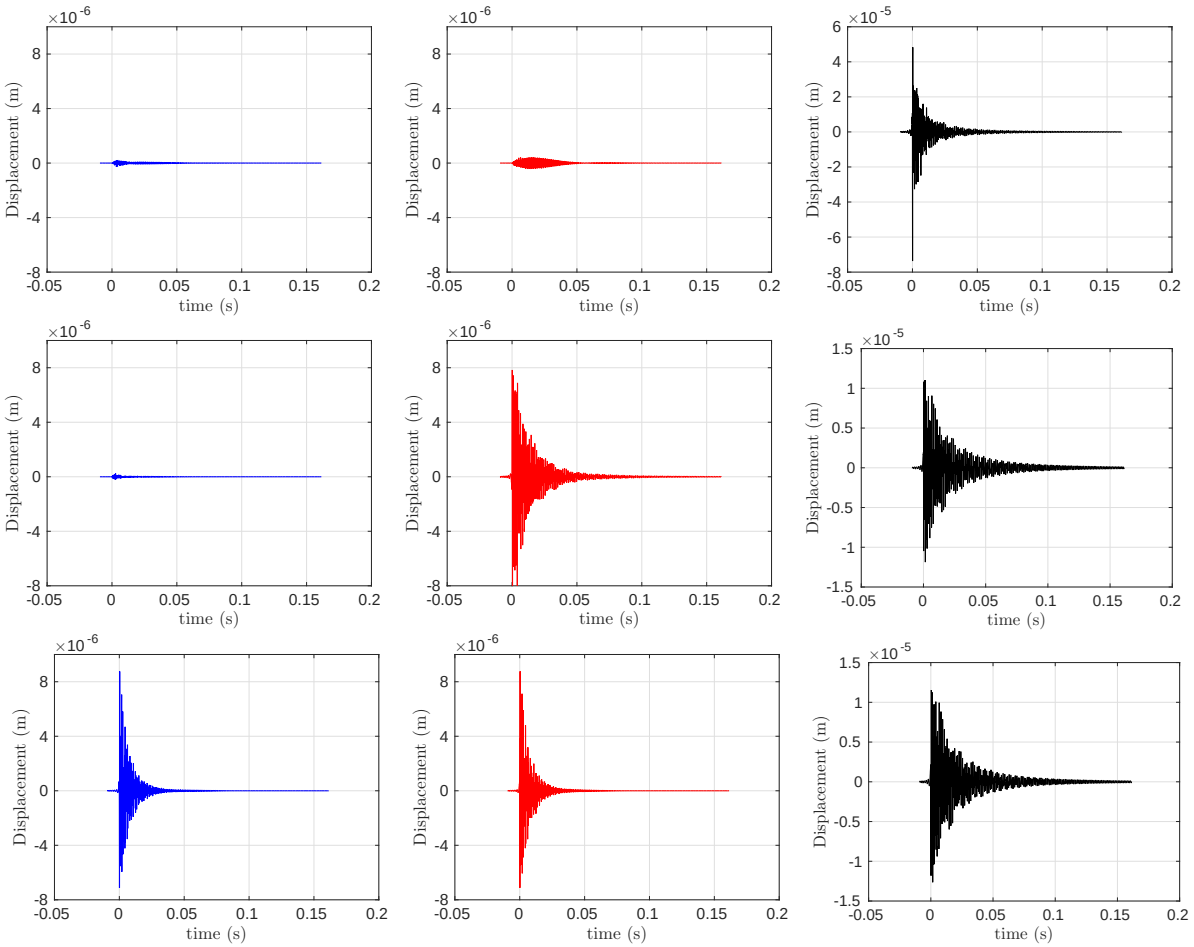

Figure 9 – Displacements $t \mapsto U^{n_{obs}^S}(t)$ of the observation points $n_{obs}^S = (1, 2, 3)$ in the structure (up,middle,bottom) along $(\mathbf{e}_x, \mathbf{e}_y, \mathbf{e}_z)$, (left,middle,right)

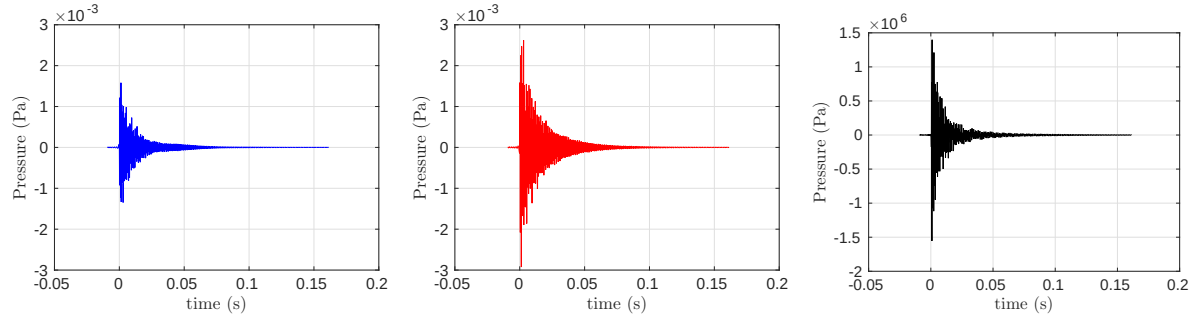

Point 1 Point 2 Point 3

Figure 10 – Pressure $t \mapsto P^{n_{obs}^F}(t)$ at the observation points $n_{obs}^F = (1, 2, 3)$ in the fluid (left, middle, right).

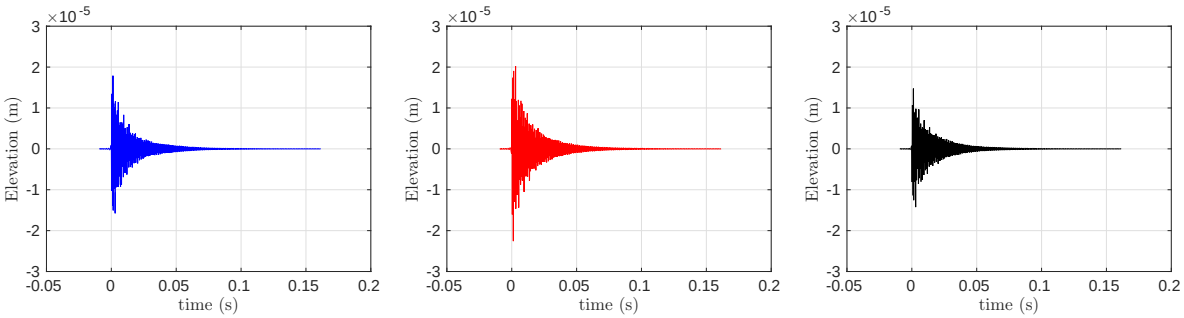

Figure 11 – Elevation $t \mapsto \mathbf{H}^{n^H_{obs}}(t)$ at the observation points on the free surface $n^H_{obs} = (1, 2, 3)$ (left, middle, right).

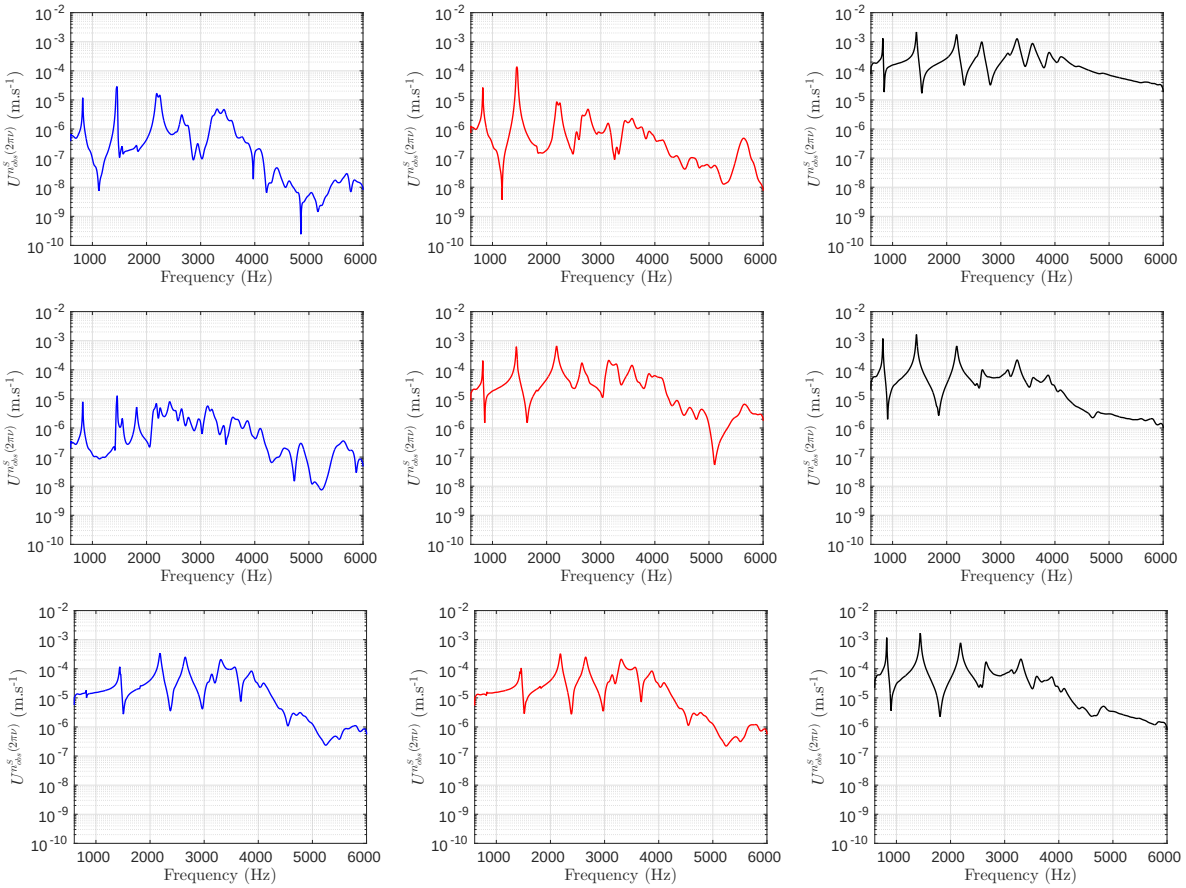

Figure 12 – Displacements $\nu \mapsto U^{n^S_{obs}}(2\pi\nu)$ of the observation points $n^S_{obs} = (1, 2, 3)$ in the structure (up,middle,bottom) along $(\mathbf{e}_x, \mathbf{e}_y, \mathbf{e}_z)$, (left,middle,right) in the frequency domain

References

[1] Paul Concus and Robert Finn. On the behavior of a capillary surface in a wedge. *Proceedings of the National Academy of Sciences of the United States of America*, 63(2):292, 1969.

[2] Franklin T. Dodge. *The "New Dynamic Behavior of Liquids in Moving Containers"*. Southwest Resear Institute, San Antonio, Texas, 2000.

[3] M El-Kamali, Jean-Sébastien Schotté, and R Ohayon. Three-dimensional modal analysis of slosh-

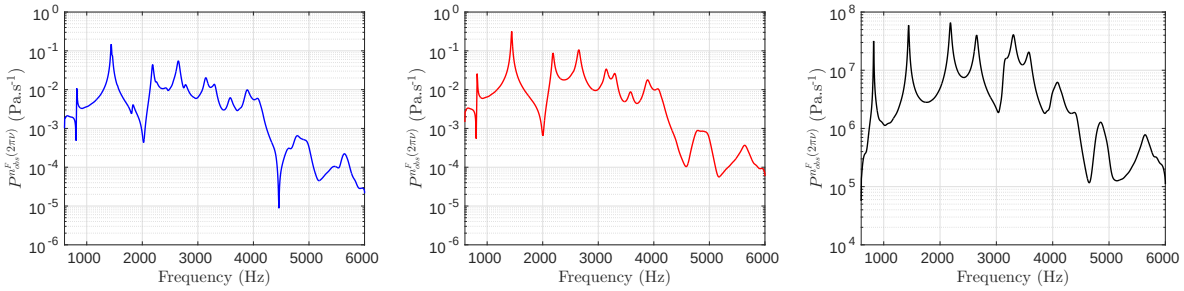

Point 1 Point 2 Point 3

Figure 13 – Pressure $\nu \mapsto P^{n^F_{obs}}(2\pi\nu)$ at the observation points $n^F_{obs} = (1, 2, 3)$ in the fluid (left, middle, right).

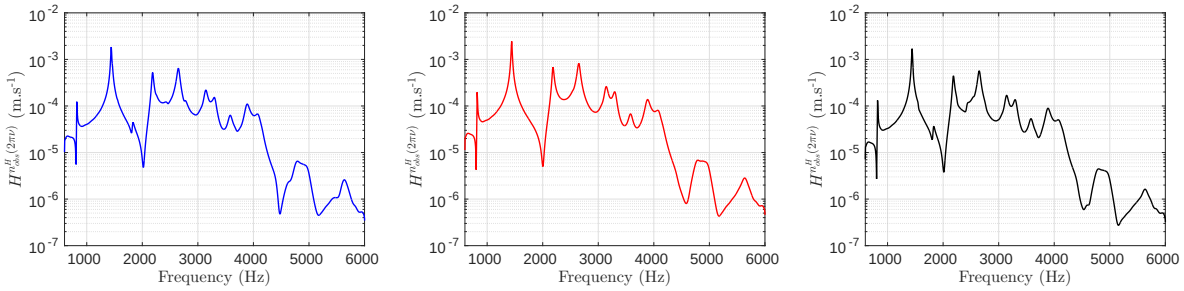

Point 1 Point 2 Point 3

Figure 14 – Elevation $\nu \mapsto H^{n^H_{obs}}(2\pi\nu)$ of the observation points $n^H_{obs} = (1, 2, 3)$ on the free surface (left, middle, right).

ing under surface tension. *International Journal for Numerical Methods in Fluids*, 65(1-3):87–105, 2011.

[4] Charbel Farhat, Edmond Kwan-Yu Chiu, David Amsallem, Jean-Sébastien Schotté, and Roger Ohayon. Modeling of fuel sloshing and its physical effects on flutter. *AIAA journal*, 51(9):2252–2265, 2013.

[5] Robert Finn. On the equations of capillarity. *Journal of Mathematical Fluid Mechanics*, 3(2):139–151, 2001.

[6] Robert Finn. The contact angle in capillarity. *Physics of Fluids*, 18(4):047102, 2006.

[7] Robert Finn and Garving K Luli. On the capillary problem for compressible fluids. *Journal of Mathematical Fluid Mechanics*, 9(1):87–103, 2007.

[8] Raouf A. Ibrahim. *Liquid Sloshing Dynamics: Theory and Applications*. Cambridge University Press, Cambridge, 2005.

[9] N. N. Moiseev and A. A. Petrov. The calculation of free oscillations of a liquid in a motionless container. *Advances in Applied Mechanics*, 9:91–154, 1966.

[10] Henri JP Morand and Roger Ohayon. *Fluid Structure Interaction*. John Wiley & Sons, New York, 1995.

[11] Roger Ohayon. Reduced models for fluid–structure interaction problems. *International Journal for Numerical Methods in Engineering*, 60(1):139–152, 2004.

[12] Roger Ohayon and Christian Soize. *Advanced computational vibroacoustics: reduced-order models and uncertainty quantification*. Cambridge University Press, New York, 2014.

[13] Roger Ohayon and Christian Soize. Vibration of structures containing compressible liquids with surface tension and sloshing effects. Reduced-order model. *Computational Mechanics*, 55(6):1071–1078, 2015.

[14] Jean-Sébastien Schotté and R Ohayon. Linearized formulation for fluid-structure interaction: Application to the linear dynamic response of a pressurized elastic structure containing a fluid with a free surface. *Journal of Sound and Vibration*, 332(10):2396–2414, 2013.